Physics Procedia

Volume 75, 2015, Pages 1158–1166

20th International Conference on Magnetism

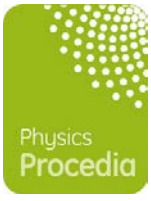

The diverse nanostructure of electroless plated CoNiFeB alloy: thin film, nanotubes and nanoparticles

D. Richardson and F. M. F. Rhen

Department of Physics and Energy, University of Limerick, Ireland

Materials and Surface Science Institute, University of Limerick, Ireland

Fernando.rhen@ul.ie

Abstract

We prepared Co-Ni-Fe-B alloys by electroless plating into porous polycarbonate membranes and investigated the formation of the nanostructure using high-resolution scanning electron microscope images and magnetic measurements. The formation of the nanostructure occurs in five stages: nucleation, particle growth, percolation, film formation and films growth. High-resolution SEM images combined with magnetic measurements reveals that the nanostructure of the deposits consists of nanotubes, nanoparticles and thin film, which is directly linked to the stages of formation. Nanotubes with various lengths were obtained with typical values between 3 to 6 μm and with wall thickness varying from 50 to 90 nm, whereas nanoparticles have average diameter up to 45 nm both depending on deposition time. The magnetic measurements show that the nanostructured $(Co_{12}Ni_{60}Fe_{28})_{88}B_{12}$ alloys have specific saturation magnetization of (88.6 ± 7.7) $JT^{-1}kg^{-1}$ for samples deposited for periods ranging from 2 to 60 min.

Keywords: electroless, nanostructure, nanotubes, magnetism, electron-microscopy

1 Introduction

Nanowires, nanotubes and nanoparticles are important nanostructures due to their application to solar cells [1,2], magnetic recording industry as nanodevices [3, 4], biomedical industry [5], microelectromechanical systems [6], electronic industries [7] and magnetic storage media [8, 9, 10]. Alloy and metals investigated in nanostructures includes nanotube of Fe_2O_3 and Fe_3O_4 for the biomedical industry [5], CoTe nanotubes applied solar cell production [1,2], nanotubes of Co, Ni, Ni-Fe, Fe-Co, [11-13], Co-Ni-Fe [14-16], Co-Pt and Fe-Pt nanotubes and nanowires for magnetic storage media [8, 9, 10, 9] and $CoFe_2O_4$ for medical/electronic industries [7]. Most reports on the preparation methods are based on template [17] to obtain the desired nanostructure. Electrodepositon [1, 14] and electroless deposition [15, 16] are the mostly used techniques to prepare nanostructures using templates.

 Selection and peer-review under responsibility of the Scientific Programme Committee of ICM 2015

doi:10.1016/j.phpro.2015.12.187

Electroless deposition requires the presence of a catalyst and it is a simple and cheap method for the preparation of metal and alloy. This method has been used for the preparation of non-magnetic nanotubes such as Cu [18] and Au [19]. Magnetic Co-Ni-Fe-B films have been prepared by Osaka and co-workers [20, 21, 22]. In recent work, we showed the preparation of electroless plated coaxial nanotubes [16]. Here, we focus our investigation on the nanostructures formation and magnetic properties of single Co-Ni-Fe-B alloy, which consist of electroless plated single wall Co-Ni-Fe-B into polycabonate membrane. In our investigation, we characterize the magnetic properties of the deposits and deposition parameters to show that the deposition of Co-Ni-Fe-B results in a nanostructure comprising nanotubes, thin film and nanoparticles.

2 Experimental

The nanostructured Co-Ni-Fe-B deposits were prepared using electroless method. Cyclosporine track etched polycarbonate membranes of 25 mm diameter with 400 nm diameter pores were used as template to study growth of Co-Ni-Fe-B deposits. The activation process consists in first fully immerging the membranes for 10 min. in 0.013 M $SnCl_2$ with 0.24 M HCl at 40 ºC, followed by 10 min. complete immersion in 1.4 x 10^{-3} M $PdCl_2$ solution at 65 ºC and then the membranes were dried at 85 ºC for 15 min.

The deposition of Co-Ni-Fe-B alloy was carried out from a solution containing 0.019 M $NiSO_4$-$6H_2O$, 0.016 M $CoSO_4$-$7H_2O$, 0.013 M $FeSO_4$-$7H_2O$, 0.052 M diammonium citrate, 0.07 M dimethylamine borane and 0.143 M lactic acid all with pH 9 at 65 ºC. After the deposition, the membranes were washed in deionized water and dried in a light flow of nitrogen gas. Deposition time was varied from 2 min to 60 min.

Magnetic measurements were carried out in as-deposited structures in the polycarbonate membranes and after membrane etching using a Lakeshore vibrating sample magnetometer (VSM) at room temperature up to a maximum applied magnetic field of 1.5 T. The deposits were imaged in the field free mode on a Hitachi SU-70 scanning electron microscope (SEM). The images were taken at an accelerating voltage of 30 kV and working distance of 5 mm. The composition of the nanotubes was determined using energy dispersive X-rays (EDX) using an Oxford Instruments X-Max attachment to the SEM. Boron content was determined using X-Rays Photoelectron Spectroscopy (XPS) model Kratos Axis 165. For imaging purposes the membranes were dissolved in concentrated KOH solution.

3 Results and discussion

The deposition of nanostructured Co-Ni-Fe-B alloys was carried out by placing polycarbonate membranes floating on solution. A visual inspection of the deposits shows changes in coloration, which indicates that the deposition occurs throughout the membrane template. The combination of EDX and XPS analysis of the deposits show a $(Co_{12}Ni_{60}Fe_{28})_{88}B_{12}$ composition.

We removed the membrane template by immersing the deposits into concentrated KOH solution. By carrying out magnetic measurements before and after the removal of the membrane, we ruled out any measurable dissolution of the Co-Ni-Fe-B deposits. Measurement of the saturation moment before and after the etching process for samples deposited for periods ranging from 5 to 20 min are identical within 2 % uncertainty. This indicates that the nanostructure does not dissolve in concentrated KOH solution during the membrane etching process.

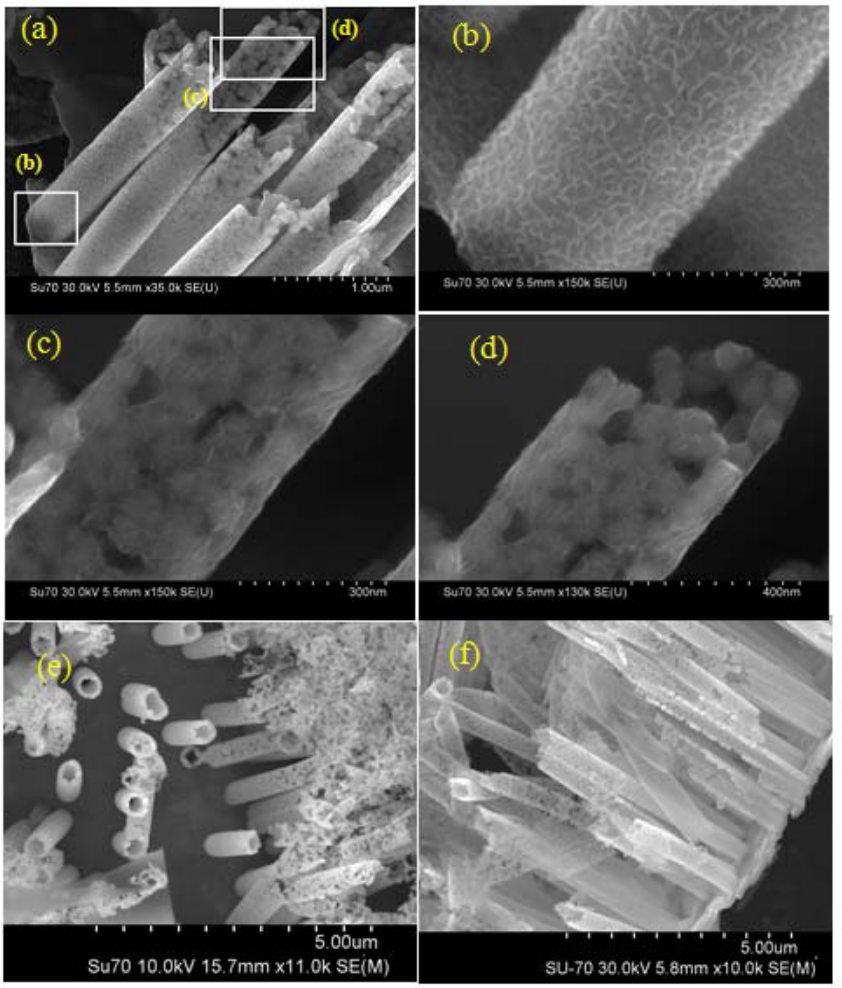

Figure 1. SEM image of nanotubes showing different stages of growth for 5 min deposits (a,b,c,d,e). (a) Image of the nanotube, (b) high resolution image showing a continuous film forming the wall of the nanotubes, (c) nanotube formation at percolation stage, (d) details of nanoparticles at the earlier stages of percolation, (e) image showing nanoparticles on top of nanotubes on 5 min deposits and (f) side image of nanotubes deposited for 10 min

We also characterized the electroless Co-Ni-Fe-B deposits using high resolution SEM images as shown in figure 1. Our analysis of the growth of the deposits is consistent with a formation of the nanostructure that can be categorized in five stages: nucleation, nanoparticle growth, percolation, film formation and films growth. During the nucleation stage Pd nanoparticles act as a catalyst allowing the formation of Co-Ni-Fe-B nanoparticles, which is immediately followed by particle growth. Nanoparticles are visible in the image presented in Fig.1(d) and Fig.1(e). As the Co-Ni-Fe-B nanoparticles grow they start to percolate with neighbouring nanoparticles and then the film formation stage begins, which is responsible for the formation of the continuous tubes, see Fig. 1(b). Finally, as

the 3-D growth of nanoparticles is suppressed due to coalescence with neighbouring particles, the 1-D growth dominates, which is final stage where the thickness of the deposits increases with time. This stage is responsible for thickening both the walls of the nanotubes and the film on the base of the membrane. We observed that the nanostructure of the deposits is very similar for deposition times ranging from 3 to 20 min. The wall thickness varies from 50 to 90 nm with nanotube length between 3 to 6 μm. An artistic illustration is presented in figure 2 showing the stages of nucleation, particle growth, percolation and film formation.

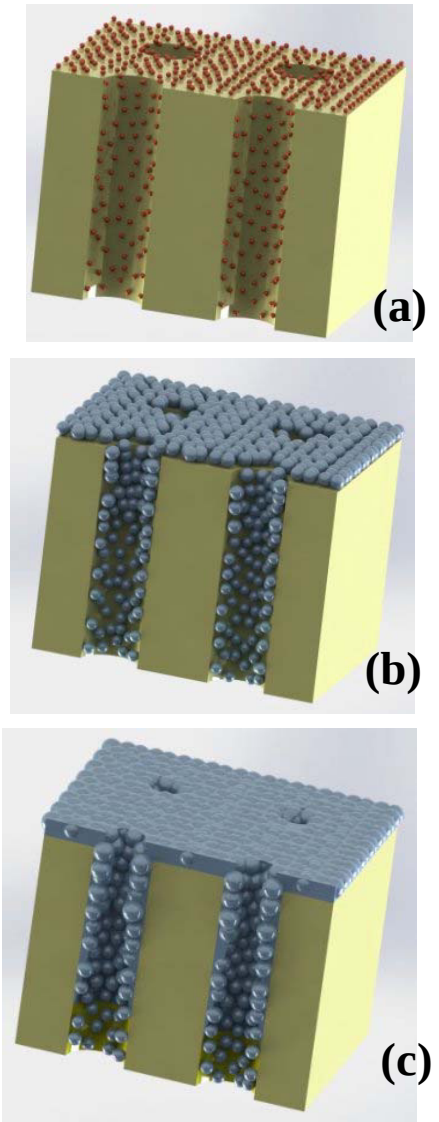

Figure 2. A 3-D artistic illustration showing different stages of growth of Co-Ni-Fe-B alloy. (a) Nanoparticles nucleating from Pd catalyst, (b) nanoparticle growth and (c) percolation and film formation.

At the film growth stage, the nanotube wall thickness varies with time as shown in fig. 3. After a 2 minute deposition the average thickness of the nanotubes is approximately 50 nm thick, Fig. 3(a). This increases to approximately 80 nm for a 5 min deposition, Fig. 3(b), and 90 nm for a 10 minutes deposition, Fig. 3(c). The reduction in deposition rate is evident from the dependence of nanotube wall thickness with time Fig. 3 (d). The main contributing factor to the reduction of the deposition rate is the reduction of the inner tube diameter, which affects the mass-transport into pores of the membrane.

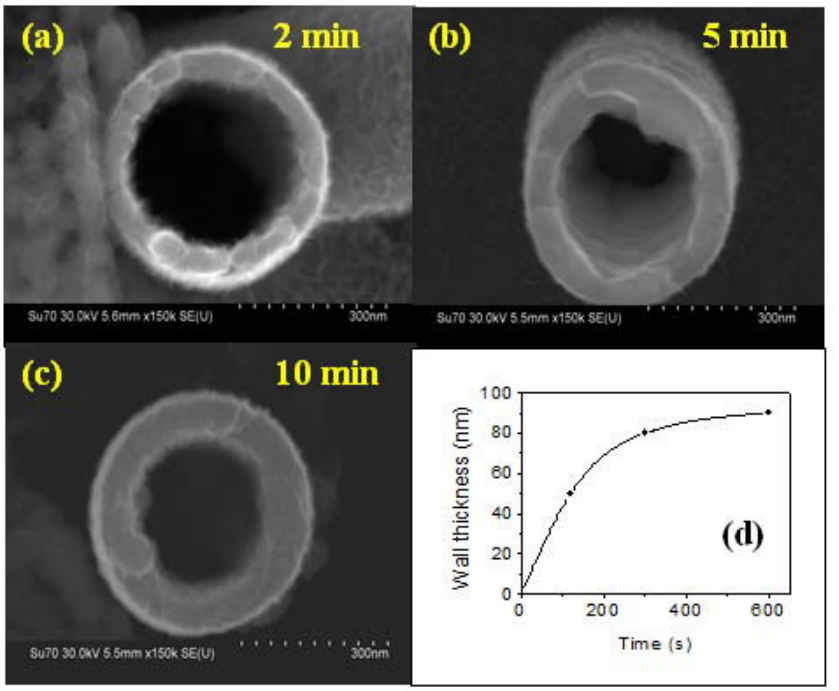

Figure 3. SEM images showing the walls of nanotubes deposited for (a) 2 min, (b) 5 min and **(c)** 10 min and (d) the dependence of wall thickness on time.

We have determined the dependence of mass per unit area on deposition time, as shown in figure 4. The error bars are obtained from propagation of uncertainty from sample size, total mass of the sample and mass of the membrane. The slope of the plot of dependence of the mass per area with the deposition time is linked to mass deposition rate. The non-zero intercept indicates that at earlier stages of the deposition the deposition rate is larger, which is consistent with fast growth of nanoparticles. As the dependence is linear, we conclude that the mass deposition rate is constant with time over a wide range of deposition times. The data at short period of time show larger relative uncertainties, as the amount of deposited material is small compared to the membrane mass. The effect of mass-transport on the growth of the nanotubes is not evident in figure 4 at first sight; as one would expect that it would be reflected on the deposition rate. This is partially due to the fact that the nanotube mass is small compared to total mass of the magnetic deposit.

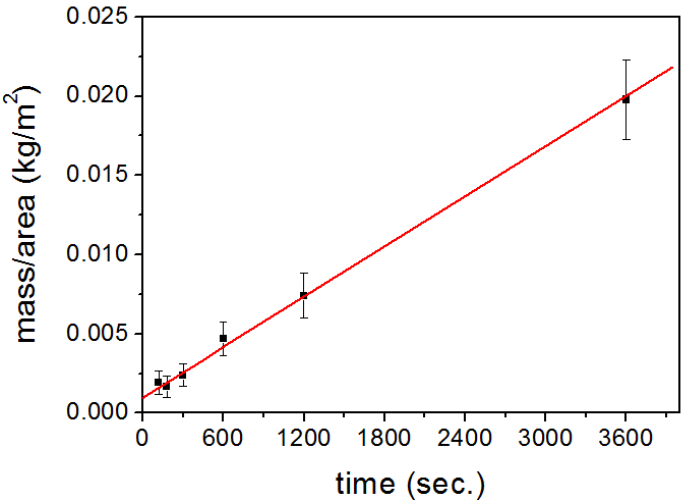

Figure 4. Dependence of mass per unit area on the deposition time. The line represents the best linear fitting of the curve using weighted least square.

Room temperature magnetic measurements in the plane of the membrane are shown in Fig. 5 and were carried out prior to the removal of the membrane. The specific saturation magnetization of the deposits is 88.6 ± 7.7 J/Tkg, at saturation applied field of 1.5 T, and does not depend on deposition time, Fig. 5 (e). Uncertainties on the specific magnetization were obtained by propagation of uncertainties from the sample mass and magnetic moment. Here, the specific saturation magnetization accounts for the contribution of three structures: thin film, nanotubes and nanoparticles. Therefore, as the deposition conditions are kept constant during the nanostructure formation the specific magnetization is as constant throughout the deposit, hence it is reasonable to the overall specific saturation magnetization would not dependent on the partial volume fractions of the nanostructures. In addition, experimental data indicating magnetization independence on time is also consistent with a structure where the volume of one sub-structure dominates in relation to the others. As this can be inferred in our case for long deposition times, where the contribution form the film on the base on the membrane dominates. Our results show that the magnetization saturation does not depend on deposition time within the uncertainties.

The shape of the magnetization curves, as shown in figure 5, represents mainly the magnetic contributions of the film and the nanotubes. We observed that the thickness of the film grows faster with time than the thickness of nanotube wall. In addition, the jump of magnetization at low applied field is associated with the switching of the magnetization direction of the film, which shows low coercivity compared to the nanotubes. Therefore as the deposition time increases, the behaviour of the magnetization curves tends to that of a film and the coercivity decreases with deposition time.

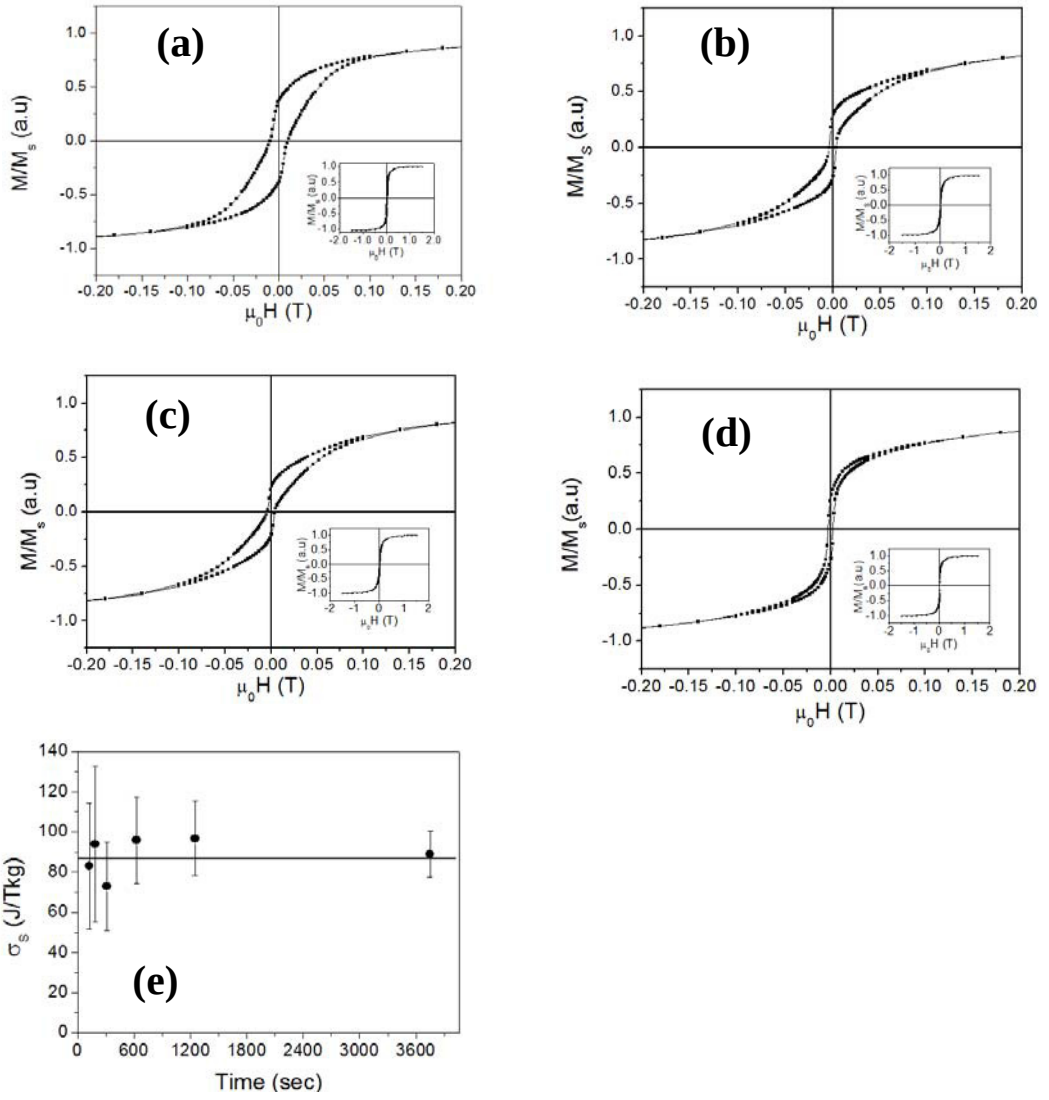

Figure 5. Room temperature normalized magnetization curves of electroless Co-Ni-Fe-B deposits plated for (a) 5 min, (b) 10 min, (c) 20 min and (d) 60 min. All measurements shown were carried out in the plane of the membrane template. The specific saturation magnetization of the deposits was obtained at an applied field of 1.5 T (e). The continuous line in (e) represents the average specific saturation magnetization value.

4 Conclusion

Our investigation reveal growth stages of nanostructured electroless plated $(Co_{12}Ni_{60}Fe_{28})_{88}B_{12}$ alloy into polycarbonate membranes. The formation of the nanostructure occurs in five stages: nucleation, particle growth, percolation, film formation and films growth. The combination of high resolution SEM imaging and magnetic measurements reveal the nanostructure of the deposits, which depends on the final stage of growth. Nanotubes and thin film are formed when the five stages are completed, whereas nanoparticles are formed at the first two initial stages of deposition, before percolation occurs. The Co-Ni-Fe-B deposits consist of a continuous film on the base of the membrane, continuous nanotubes and nanoparticles deposited on the walls the pores. Nanotubes with various lengths were obtained with typical values between 3 to 6 μm in our investigation. The magnetic measurements show that the nanostructures have a specific saturation magnetization is (88.6 ± 7.7) $JT^{-1}kg^{-1}$. These nanostructures may find application in sector of energy.

5 Acknowledgements

We also would like to thank Science Foundation Ireland (12/IP/1692) and IRCSET (RS/2011/270) for financial support.

6 References

[1] R.R. Shi, X.H. Liu, Y.G. Shi, R.Z. Ma, B.P. Jia, H.T. Zhang, G.Z. Qiu, J. Mater. Chem. **20,** 7634 (2010)

[2] J. Li, X.S. Tang, L.X. Song, Y.C. Zhu, Y.T. Qian, J. Cryst. Growth **311**, 4467 (2009).

[3] R. Sharif, S. Shamaila, M. Ma, L.D. Yao, R.C. Yu, X.F. Han, M. Khaleeq-ur-Rahman, Appl. Phys. Lett. **92,** 032505 (2008)

[4] K. M. Razeeb, F. M. F. Rhen, S. Roy, J. Appl. Phys. **105**, 083922 (2009).

[5] L. F. Chen, J. N. Xie, K.R. Aatre, V.K. Varadan, Journal of Nanotechnology in Engineering and Medicine **1,** 011009 (2010)

[6] F. M. F. Rhen, E. Backen, J. M. D. Coey, J. Appl. Phys. **97**, 113908 (2005).

[7] J. C. Fu, J.L. Zhang, Y. Peng, J.G, Zhao, G.G. Tan, N.J. Mellors, E.Q. Xie, W.H Han, Nanoscale. **4**, 3932 (2012)

[8] H.R. Liu, Q.F. Lu, X.F. Han, X.G. Liu, B.S. Xu, H.S. Jia, Appl. Surf. Sci. **258,** 7401 (2012)

[9] Y.H. Huang, H. Okumura, G.C. Hadjipanayis, D. Weller, J. Appl. Phys. **91,** 6869 (2002)

[10] Y.C. Sui, R. Skomski, K.D. Sorge, D.J. Sellmyer, Appl. Phys. Lett. **84,** 1525 (2004)

[11] M. Daub, M. Knez, U. Goesele, K. Nielsch, J. Appl. Phys. **101,** 09J111 (2007)

[12] X.F. Han, S. Shamaila, R. Sharif, J.Y. Chen, H.R. Liu, D.P. Liu, Adv. Mater. **21,** 4619 (2009)

[13] F.S. Li, D. Zhou, T. Wang, Y. Wang, L.J. Song, C.T. Xu, J. Appl. Phys. **101,** 014309 (2007)

[14] F.E. Atalay, H. Kaya, V. Yagmur, S. Tari, S. Atalay, D. Avsar, Appl. Surf. Sci. **256,** 2414 (2010)

[15] A. Azizi, M. Mohammadi, S.K. Sadrnezhaad, Mater. Lett. **65,** 289 (2011)

[16] J.F. Rohan, D.P. Casey, B.M. Ahern, F.M.F Rhen, S. Roy, D. Fleming, S.E. Lawrence, Electrochem. Comm. **10,** 1419 (2008)

[17] C.R. Martin, L.S. VanDyke, Z. H.Cai, W. B. Liang, J. Am. Chem. Soc. **112,** 8976 (1990)

[18] T. Chowdhury, D.P. Casey, J.F. Rohan, Electrochem. Comm. **11,** 1203 (2009)

[19] M. Wirtz, C.R. Martin, Adv. Mater, **15,** 455 (2003)

[20] T. Homma, Y. Sezai, T. Osaka, Electrochim. Acta **42**, 3041 (1997)

[21] T. Yokoshima, D. Kaneko, M. Akahori, H.S. Nam, T. Osaka, J. Electroanal. Chem. **491,** 197 (2000)

[22] T. Yokoshima, S. Makamura, D. Kaneko, T. Osaka, S. Takefusa, A. Tanaka, J. Electrochem.Soc. **149**, C375 (2002)